International Journal of Fluids Engineering.
ISSN 0974-3138 Volume 5, Number 1 (2013), pp. 1-20

http://www.irphouse.com

A CFD Analysis of Turbulent Fluid Flow in Closed and Semi-Closed Porous Enclosure

Snehamoy Majumder[1], Debajit Saha[2] and Pritam Das[2]

[1]Associate Professor, Department of Mechanical Engineering, Jadavpur University, Kolkata- 700 032, West Bengal, India
[2]Research Scholar, Department of Mechanical Engineering, Jadavpur University, Kolkata- 700 032, West Bengal, India
Email: srg_maj@yahoo.com

ABSTRACT

The CFD analysis of the turbulent fluid flow through an axi-symmetric circular duct with side mass injection through the porous wall with closed inlet as well as partially opened inlet, have been carried out by using modified $\kappa-\varepsilon$ model, considering streamline curvature effects by modifying the model constants. The flow patterns of the fluid have been investigated for various side injection velocities with different ratio of inlet opening radius (r_i) to the external radius (r_o) of the duct. This ratio has been varied as 0.1, 0.2, 0.3, 0.4 and 0.5 to visualize the change of the flow pattern and the size of the recirculatory flow due to the partial opening with mass injection through the porous wall of the duct. It has been observed that in a partially opened circular duct with the increase of this ratio, the size of the recirculation generated at inlet gradually decreases at a constant side injection velocity. And the recirculation bubble gradually increases with the increase of the injection velocity in a closed circular duct.

Keywords: Closed inlet and partially opened inlet, Side mass injection, Porous wall, streamline curvature, Recirculatory flow, Ratio of inlet opening radius (r_i) to the external radius (r_o).

INTRODUCTION

The side mass injection flow allowed normally or at an angle into a main turbulent bulk flow occurs in various industrial processes. To get better

performance in a Gas Turbine combustor, mixing of air entering through the liner holes with high temperature combustion gasses is very much required to provide a more uniform temperature pattern at the outlet of the combustor to be compatible to the Turbine blades. The degree and rate of the mixing process is important in combustion applications because the burning efficiency and the exhaust composition depend on mass transfer. Several researchers have done theoretical, numerical and experimental works in this field studying parameters that include the penetration and mixing characteristics of cross turbulent flows. In most of the works the main duct fluid flow has been considered along with the side mass injection. In the present investigations we consider two cases. In the first case there is no main flow only the side mass injection is present. Where as in the second case a partial main flow along with the side mass injection have been considered.

Yuan and Brogren [1] theoretically investigated an isothermal flow in a porous wall pipe with fluid injection or suction at the wall. The axial velocity distribution has been expressed as functions of velocity through the porous wall, the axial pressure gradient and the mixing length proportionally constant.

Barcilon and Curtet [2] experimentally found that the Craya-Curtet number is an important parameter for characterizing the re-circulation zones that are often associated with mixing of jets. The numerical investigation of destabilization of the flow in a cylindrical duct has been reported by using the modification of standard model for streamline curvature by Launder and Spalding [4].

Beddini [7] performed numerical studies of the injection-driven flow in a duct using a parabolic form of the Navier-Stokes equations together with a full Reynolds stress turbulence model. The results indicate that the flows in a porous tubes at large injection Reynolds number can undergo three regimes of flow development. It includes the velocity field development with laminar velocity theory, high levels of turbulence development and the transition of the mean axial distribution which occurs at extremely high injection Reynolds number.

Sumitani and Kasgai [8] performed direct numerical simulation of the fully developed two dimensional turbulent channel flows with uniform wall injection and suction between two isothermal walls. They showed that the velocity and temperature fluctuations, the Reynolds shear stress and the turbulent heat fluxes increases with injection and decreases with suction. The injection stimulates the occurrence of the quasicoherent stream wise vertical structures whereas the suction suppresses these activities.

Casalis *et al.* [9] have shown that the flow induced by incompressible fluid injection through porous walls of a channel is intrinsically linearly unstable. The analytical laminar solution in a self similar form of such a motion has been calculated by Taylor in the case of an inviscid flow, the so-called ‘‘Taylor flow.’’ To develop two heterogeneous phases in the flow, particles are released in the fluid by the lateral walls during the combustion. Feraille and Casalis [11] studied the influence of these particles on stability with stability

results from the single-phase studies.

Ali *et al.* [10] studied the supersonic mixing of flow fields with three different inlet configurations by solving two-dimensional full Navier-Stokes equations. Non-reacting analysis showed that for the main flow of high Mach numbers the upstream recirculation region is responsible for enhanced mixing efficiency, as mixing occurs mostly at that region.

A large eddy simulation has been performed by Apte and Yang [12] to investigate the flow development in a porous walled chamber with surface mass injection. The flow field is characterized by three distinct regimes: laminar, transitional and fully developed turbulent flows. Surface injection prohibits deep penetration of outer fluid close to the wall which leads to the formation of coherent vortices in the mid section. With the increase of axial velocity it overcomes the effect of mass injection in further downstream by the formation of three dimensional eddies.

Knikker et *al.* [13] numerically studied the effects of buoyancy generated by wall injection in a channel flow. Fluid was injected with uniform velocity through a porous horizontal wall into the channel, closed on one side by an adiabatic wall. They observed that with weak buoyancy force the flow is steady and a recirculation appeared in the upper corner zone. They observed that with increase of the buoyancy effect the size of the recirculation zone increases.

Fournier et *al.* [15] experimentally investigated the internal flow in a channel induced by radial injection through porous wall. It has been observed that the flow structure varies depending on the porosity of the plate material used for the investigation. Flows generated by wall injection involve two basic characteristics. The main features of such flows are the strong curvature of the streamlines and the accelerated flow in the downstream direction.

In the present analysis the flow pattern and velocity distribution at various location have been observed with the variation of the injection velocity of side mass injection through the porous wall and the ratio of the inlet opening radius to the external radius of the duct. The flow has been considered to be steady, turbulent, incompressible and non-reacting. The control volume formulation of Patankar [6] using power law scheme with SIMPLER algorithm has been employed for the analysis. The $\kappa - \varepsilon$ equations have been solved with the assistance of wall function. It has been noticed that the starting of recirculation as well as the variation of length and breadth of the recirculation bubble strongly depends on the side injection and on the opening of the inlet of the circular duct.

GEOMETRICAL DESCRIPTION

Fig. 1 shows the essential features of the axi-symmetric turbulent fluid flow through circular duct closed at inlet, which has been considered with entries in the duct from radial directions through the porous wall. There is no main flow through the duct and as the inlet of the duct is closed so it has been

considered as a wall and the wall boundary conditions (no slip) has been applied at the inlet in the present analysis. The cylindrical coordinate $r-\theta-x$ has been considered. However the azimuthal component is absent owing to the fact that the geometry as well as the boundary conditions is axi-symmetric. The side injection velocity has been denoted by V_{inj}.

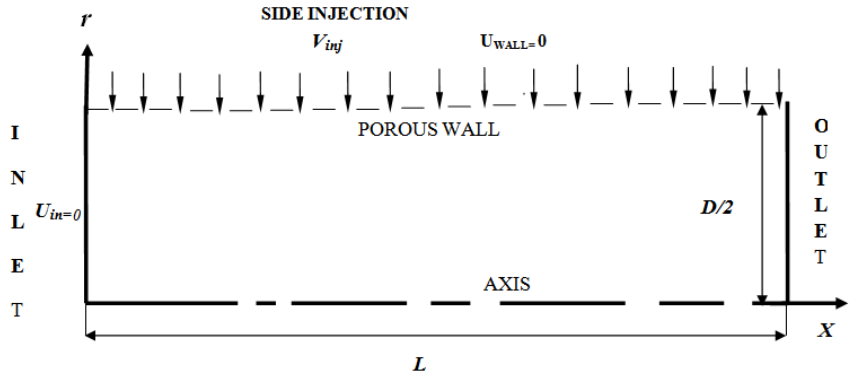

Figure 1, Schematic diagram of the axi-symmetric circular duct with side injection through porous wall and closed inlet.

Fig. 2 shows the essential features of the axi-symmetric turbulent fluid flow through a partially opened enclosure, which has been considered with entries in the duct from radial directions through the porous wall. In the present analysis the inlet opening radius has been varied to investigate the flow pattern in the axi-symmetric circular duct.

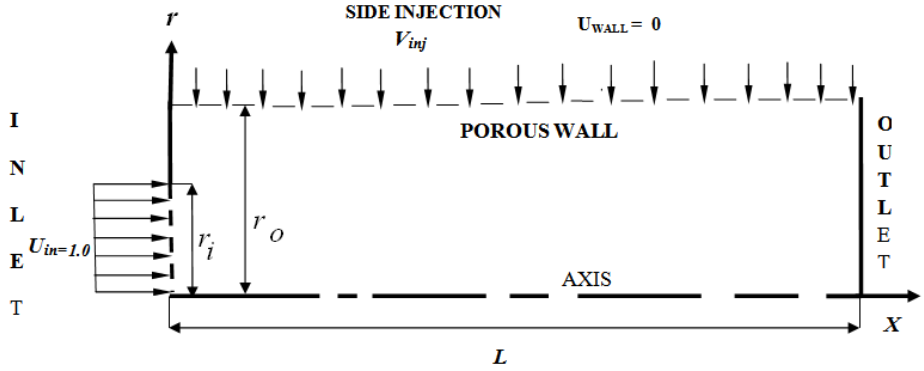

Figure 2, Schematic diagram of the axi-symmetric circular duct with side injection through porous wall and partially opened inlet

For the present findings the following nomenclature has been taken,
The axial length of the duct is considered as L = 9 m.
The diameter of the duct is considered as D= 0.1534 m.
Air density, ρ = 1.235 kg/m^3.

Molecular viscosity of air, $\mu_l = 1.853\times10^{-5}$kg/m.s.

Reynolds number, $Re = (\rho\ U_{mean}\ D)/\mu_l$. where U_{mean} is the mass-averaged axial inlet velocity.

$\frac{r_i}{r_o}$ ratio has been varied as 0.1, 0.2, 0.3, 0.4 and 0.5.

MATHEMATICAL MODELING

The mass and momentum conservation equations in axi-symmetric cylindrical co-ordinate system for the turbulent mean flow with eddy viscosity model is given as follows:

3.1. Governing Equations

3.1.1. Continuity Equation

$$\frac{\partial(\rho\bar{u})}{\partial x} + \frac{1}{r}\frac{\partial(\rho r\bar{v})}{\partial r} = 0 \tag{1}$$

3.1.2. MOMENTUM EQUATIONS

AXIAL COMPONENT (X-COMPONENT)

$$\rho\left[\bar{v}\frac{\partial\bar{u}}{\partial r} + \bar{u}\frac{\partial\bar{u}}{\partial x}\right] = -\frac{\partial\bar{p}}{\partial x} + \frac{\partial}{\partial x}\left(\mu_{eff}\ \frac{\partial\bar{u}}{\partial x}\right) + \frac{1}{r}\frac{\partial}{\partial r}\left(r\mu_{eff}\ \frac{\partial\bar{u}}{\partial r}\right) + \left[\frac{\partial}{\partial x}\left(\mu_{eff}\ \frac{\partial\bar{u}}{\partial x}\right) + \frac{1}{r}\frac{\partial}{\partial r}\left(r\mu_{eff}\ \frac{\partial\bar{v}}{\partial x}\right)\right] \tag{2}$$

RADIAL COMPONENT (R-COMPONENT)

$$\rho\left[\bar{v}\frac{\partial\bar{v}}{\partial r} + \bar{u}\frac{\partial\bar{v}}{\partial x}\right] = -\frac{\partial\bar{p}}{\partial r} + \frac{\partial}{\partial x}\left(\mu_{eff}\ \frac{\partial\bar{v}}{\partial x}\right) + \frac{1}{r}\frac{\partial}{\partial r}\left(r\mu_{eff}\ \frac{\partial\bar{v}}{\partial r}\right) + \left[\frac{\partial}{\partial x}\left(\mu_{eff}\ \frac{\partial\bar{u}}{\partial r}\right) + \frac{1}{r}\frac{\partial}{\partial r}\left(r\mu_{eff}\ \frac{\partial\bar{v}}{\partial r}\right)\right] - 2\mu_{eff}\ \frac{\bar{v}}{r^2} \tag{3}$$

Where, $\bar{u}$ and $\bar{v}$ are the mean velocity components along x and r directions respectively.

The effective viscosity is given as,

$$\mu_{eff} = \mu_l + \mu_t \tag{4}$$

Where, μ_l and μ_t are molecular or laminar viscosity and eddy or turbulent viscosity respectively.

The eddy viscosity is given by,

$$\mu_t = \rho C_\mu \kappa^2 / \varepsilon$$

Where, C_μ is an empirical co-efficient.

It is necessary to make some modifications to the constant C_μ to include

the streamline curvature effect. In the investigation the modification is taken from the concept given by Leschziner and Rodi [5] and successfully used by Majumder and Sanyal [14].

The modified form of the empirical constant C_μ is given

$$C_\mu = \frac{-K_1 K_2}{\left[1 + 8K_1^2 \frac{k^2}{\varepsilon^2}\left(\frac{\partial U_S}{\partial n} + \frac{U_S}{R_C}\right)\frac{U_S}{R_c}\right]} \tag{5}$$

Here, $U_S = \sqrt{\bar{u}^2 + \bar{v}^2}$

3.2 Turbulence $k-\varepsilon$ Model

The $k-\varepsilon$ equations are given by,

3.2.1. $k-$ Equation

$$\rho\left[\bar{u}\frac{\partial k}{\partial x} + \bar{v}\frac{\partial k}{\partial r}\right] = \frac{\partial}{\partial x}\left[\left(\mu_l + \frac{\mu_t}{\sigma_k}\right)\frac{\partial k}{\partial x}\right] + \frac{1}{r}\frac{\partial}{\partial r}\left[r\left(\mu_l + \frac{\mu_t}{\sigma_k}\right)\frac{\partial k}{\partial r}\right] + \rho G - \rho\varepsilon \tag{6}$$

Where, G is the production term and given by:

$$G = \mu_t\left[2\left\{\left(\frac{\partial \bar{v}}{\partial r}\right)^2 + \left(\frac{\partial \bar{u}}{\partial x}\right)^2 + \left(\frac{\bar{v}}{r}\right)^2\right\} + \left(\frac{\partial \bar{u}}{\partial r} + \frac{\partial \bar{v}}{\partial x}\right)^2\right]$$

The production term shows the transfer of kinetic energy from the mean flow to the turbulent motion through the interaction between the turbulent fluctuations and the mean flow velocity gradients.

3.3.2. $\varepsilon-$Equation

$$\rho\left[\bar{u}\frac{\partial \varepsilon}{\partial x} + \bar{v}\frac{\partial \varepsilon}{\partial r}\right] = \frac{\partial}{\partial x}\left[\left(\mu_l + \frac{\mu_t}{\sigma_\varepsilon}\right)\frac{\partial \varepsilon}{\partial x}\right] + \frac{1}{r}\frac{\partial}{\partial r}\left[r\left(\mu_l + \frac{\mu_t}{\sigma_\varepsilon}\right)\frac{\partial \varepsilon}{\partial r}\right] + C_{\varepsilon 1} G \frac{\varepsilon}{k} - C_{\varepsilon 2}\frac{\varepsilon^2}{k} \tag{7}$$

Here, $C_{\varepsilon 1}, C_{\varepsilon 2}, \sigma_k$ and σ_ε are the empirical turbulence constants, and some typical values of these constants in the standard $\kappa-\varepsilon$ model are recommended by Launder and Spalding which are given below-

$C_{\varepsilon 1} = 1.44$ $C_{\varepsilon 2} = 1.92$

$\sigma_k = 1.0$ $\sigma_\varepsilon = 1.3$

The standard wall function has been adopted from Launder and Spalding [4] for the solution of the $k-\varepsilon$ equations for the problem investigated here.

4. RESULTS AND DISCUSSIONS

4.1 Validation of the Present Numerical Method

In fig. 3 the present numerical method has been validated with the benchmark experimental work of Olson and Eckert [3] for turbulent flow in a porous circular tube with uniform fluid injection through the tube wall. Fig. 3(a) shows the profile of axial velocity along the radius of the porous tube at an axial distance of X/D = 10 with side mass injection through the porous wall and no flow at inlet. In Fig. 3(b) the profile of the radial velocity component has been shown at X/D = 12 in a porous circular tube with closed inlet. Figure 3(c) shows the axial velocity profiles along the radius of the porous tube at X/D=10 with a velocity ratio of side mass injection to the inlet fluid flow, Vinj/Uin = 0.0119. The approaching flow is fully developed turbulent flow. U is the mean temporal velocity in x-direction. The results include the experimental results of Olson and Eckert [3]. The matching of the experimental result with the present numerical method is quite good and the close agreement observed clearly validates the numerical scheme employed here to study the flow through a porous circular duct with closed and partially opened inlet.

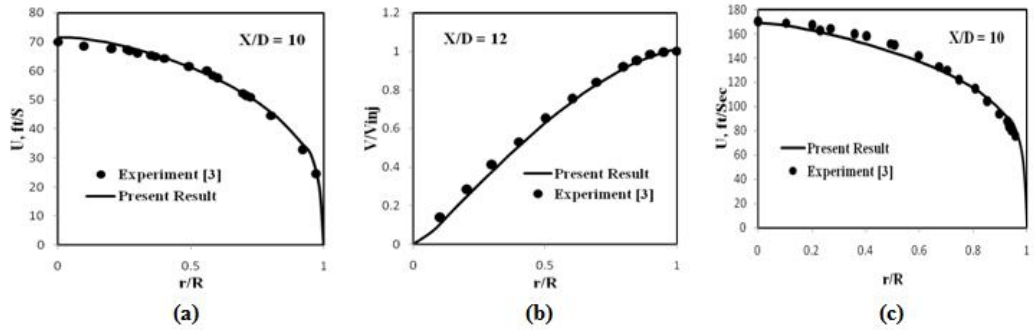

Figure 3, Validation of the present numerical method with the experimental Results [3].

4.2 Variation of the Side Injection Velocity in a Closed Enclosure

The effect of side mass injection through the porous wall of a circular tube with no flow at inlet has been shown in fig. 4. The flow pattern of the fluid along with the variation of the recirculation generated in the tube has been observed through the flooded streamline contour along with the vector diagram. Flow pattern has been investigated with zero entrance velocity at the upstream end of the porous tube so that the flow developed in the tube exclusively as a result of uniform mass injection through the tube wall. Due to the side mass injection a circulation has been formed at the upstream corner of the duct and

it has been observed that the length of the recirculation bubble gradually increases with the increase of the injection velocity through the wall of the duct. As the inlet is totally closed and due to the resistance offered to the side mass fluid by this closed inlet, there is a drop in pressure near the inlet of the duct which terminates into a low velocity flow reversal zone. The ultimate consequence is the generation of the recirculation bubble. The side mass injection velocity has been varied as 0.1 m/s, 0.2 m/s, 0.3 m/s, 0.4 m/s, 0.5 m/s and 1.0 m /s. When the injection velocity is 0.1 m/s, the breadth of the recirculation bubble reaches up to the axis of the duct and with the increase of the injection velocity the length gradually increases whereas the breadth remain same.

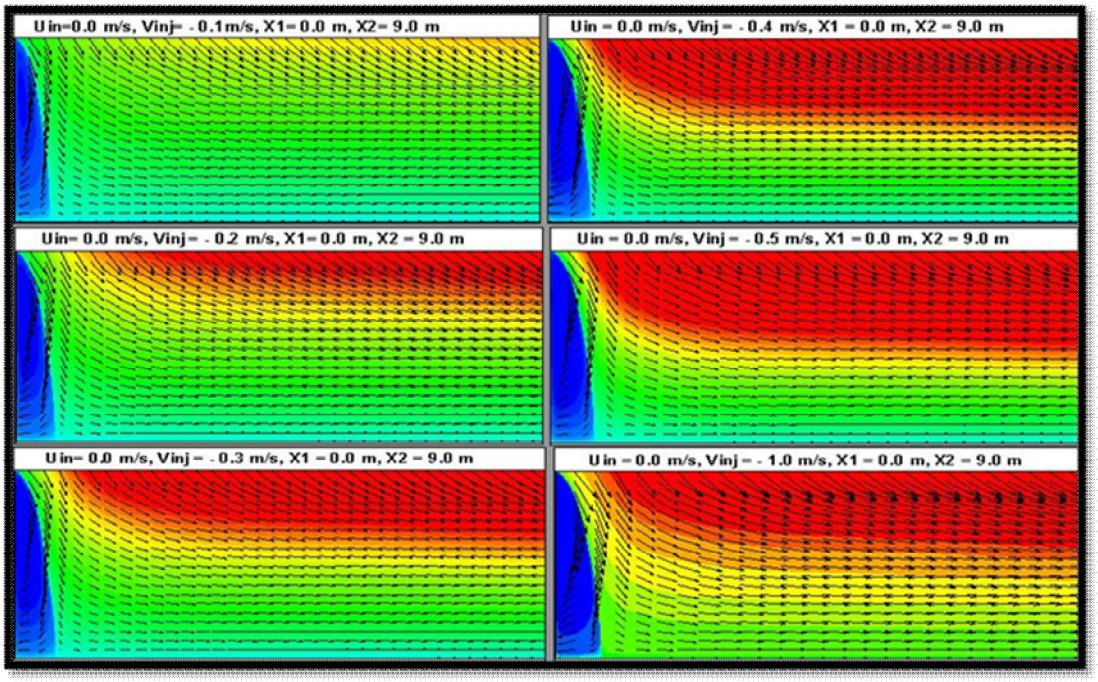

Figure 4, Variation of the flow pattern with the changes of side injection velocity (Closed enclosure).

Fig. 5 shows the variation of non-dimensional length of the recirculation bubble with the variation of side injection velocity through the porous wall. From the figure it is evident that the increment of the length of the bubble is quite remarkable up to injection velocity of 0.3 m/s. Beyond this velocity the increment in length is quite less and the recirculation bubble maintains an almost constant length.

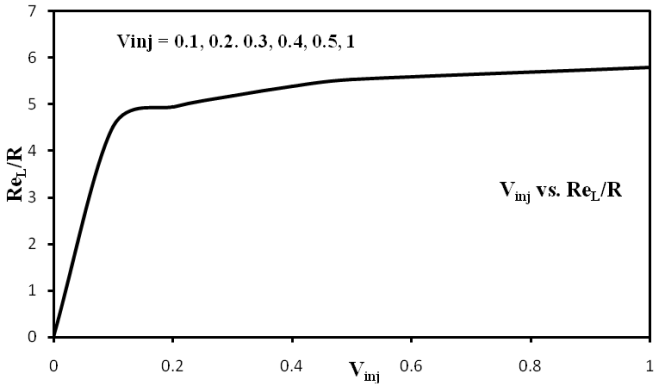

Figure 5, Variation of the recirculation length with side injection velocity.

The profiles of the axial velocities have been plotted along the radius of the duct in fig. 6 at various axial locations and at various injection velocities. Fig 6(a), 6(b) and 6(c) shows the velocity profiles at an axial distance of X = 0.34 m, X = 0.39 m and X = 0.42 m respectively. From all the plots it is evident that with the increase of the injection velocity the variation of the velocity profiles indicates the increase of the size of recirculation bubble. The axial velocity profiles gradually become positive towards downstream direction. At an axial distance of X= 0.42 m, only when the injection velocity is -1.0 m/s, the velocity profiles shows the presence of the reversal zone. At this location when the injection velocity is -0.1 m/s, -0.2 m/s, -0.3 m/s, -0.4 m/s and -0.5 m/s, the velocity profiles shows the absence of the recirculation. At X = 0.34 m. when the injection velocity is -1.0 m/s, the maximum negative value of axial velocity is above 5 m/s whereas at X = 0.39 m, its value reduces to below 5 m/s. The velocities are negative near the axis of the duct and gradually gain positive value towards the wall of the duct. From these velocity profiles it can be said that the size of the recirculation bubble gradually increases with injection velocity and the recirculation stays near the closed inlet only.

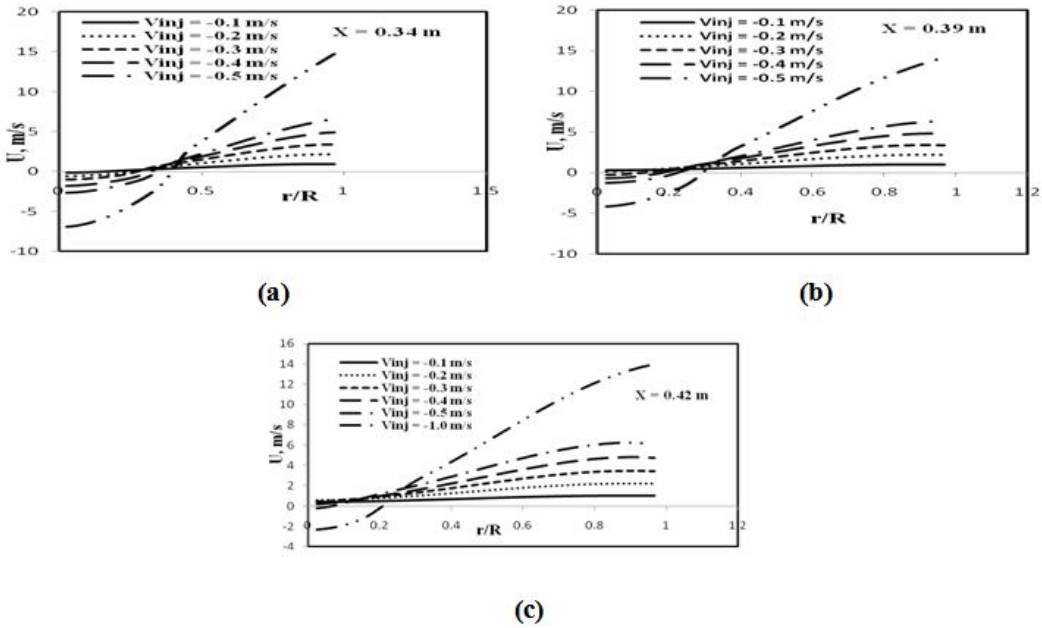

Figure 6, Velocity Profiles in porous tube (closed inlet) at Different Axial Location and Injection Velocity.

4.3 Variation of the Ratio of Inlet Opening Radius to External Radius in a partially opened Enclosure

In this section the analysis have been done in a partially opened duct with side mass injection through the porous wall. The inlet has been opened partially from the axis of the duct and the flow pattern has been investigated in such condition. The inlet opening has been defined as a ratio of inlet opening radius (r_i) to the external radius of the duct (r_o). This ratio has been varied as 0.1, 0.2, 0.3, 0.4, and 0.5. Along with this variation of this ratio the injection velocity has also been varied to analyze the effect of side mass injection on the main turbulent fluid flow entering into the porous circular duct through the partially opened inlet.

4.3.1 Side Injection Velocity (V_{inj}) = - 0.01 m/s

Keeping the side injection velocity as -0.01m/s, the ratio of Inlet Opening Radius to External radius (r_i / r_o) has been varied to analyze the variation of flow pattern in fig. 7. The velocity inlet is 1.0 m/s. It has been shown that when there is no flow at inlet a recirculation generated at the inlet and the breadth of this recirculatory flow reaches up to the axis of the duct. As the inlet opening increases the size of the recirculation gradually decreases. The length and breadth of the recirculatory flow decreases with the increase of r_i / r_o ratio. When this ratio is 0.3, the recirculation almost detaches from the wall. The recirculatory flow almost disappears when this ratio is 0.4 and 0.5.

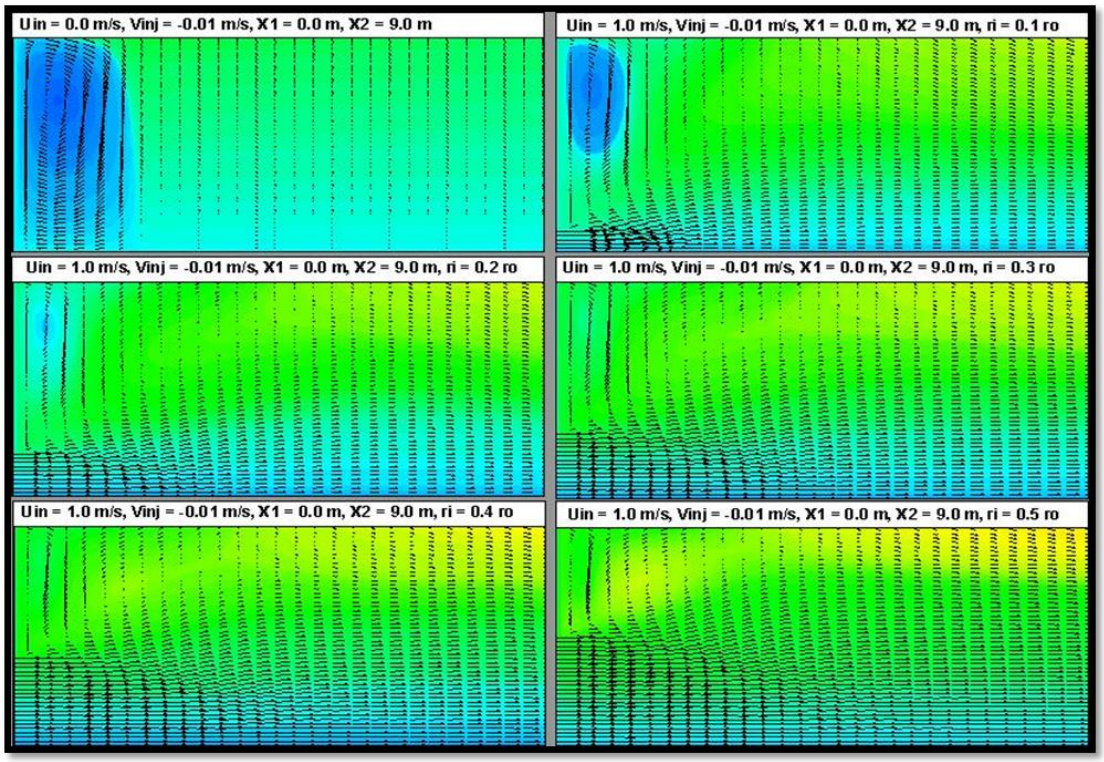

Figure 7, Variation of the Flow Pattern with the Changes of the Ratio of Inlet Opening Radius to the External Radius (Constant Side Injection Velocity, $V_{inj} = \mathbf{0.01} m/s$).

Fig. 8 shows the axial velocity profiles at X= 0.015 m and X = 0.055 m at various ratio of inlet opening to external radius. In the partially opened duct at X = 0.015 m, the axial velocities have positive value at axis and negative at the wall which confirms the presence of the recirculation bubble, whereas at X =0.055 m the velocity profiles become positive near the wall. Thus, it can be said that the reversal zone gradually decreases in length and breadth.

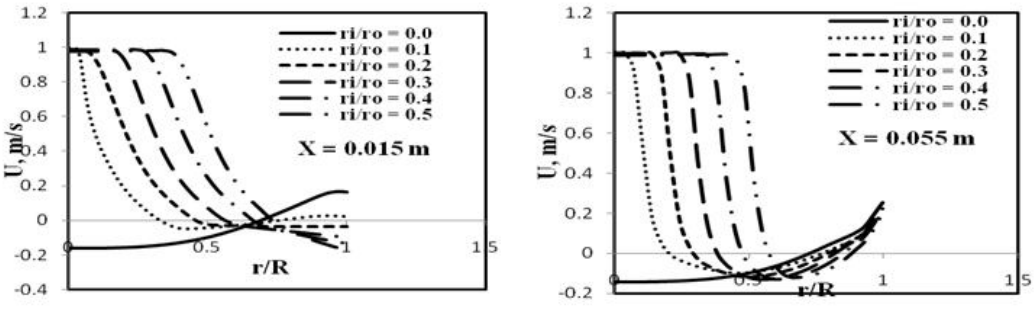

Figure 8, Velocity Profiles at Different Ratio of Inlet Opening Radius to External Radis (Side Injection velocity $V_{inj} = \mathbf{0.01} m/s$).

4.3.2 Side Injection Velocity (V_{inj}) = -0.02 m/s

In fig. 9, the flow pattern of the turbulent fluid flow through a porous circular duct with injection velocity of -0.02 m/s and inlet turbulent fluid flow at a velocity of 1.0 m/s has been shown through flooded stream contour and vector diagram. The ratio of inlet opening radius (r_i) to the external radius of the duct (r_o) has been varied. Likewise the previous case, with the increase of r_i / r_o ratio, the recirculation size decreases and it shifts from the inlet of the duct. The velocity profiles in fig. 10(a) and 10(b) shows the same variation of the recirculation bubble.

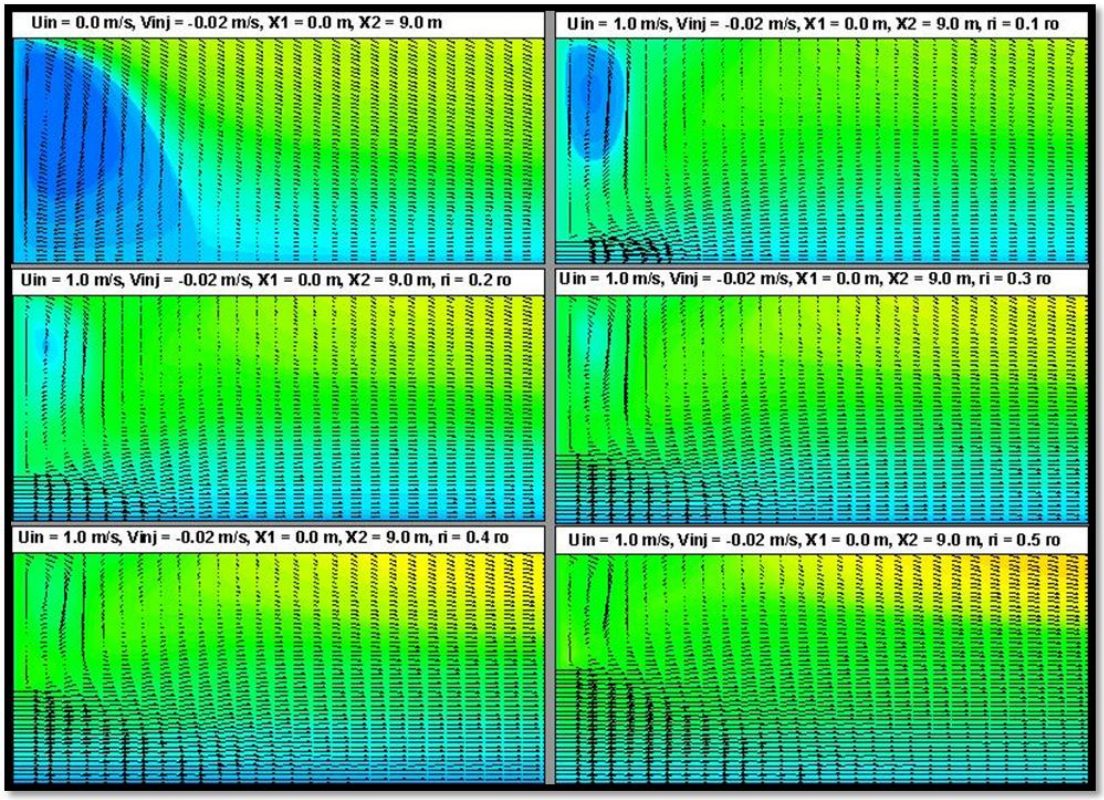

Figure 9, Variation of the Flow Pattern with the Changes of the Ratio of Inlet Opening Radius to the External Radius (Constant Side Injection Velocity, $V_{inj} = \mathbf{0.02} m/s$).

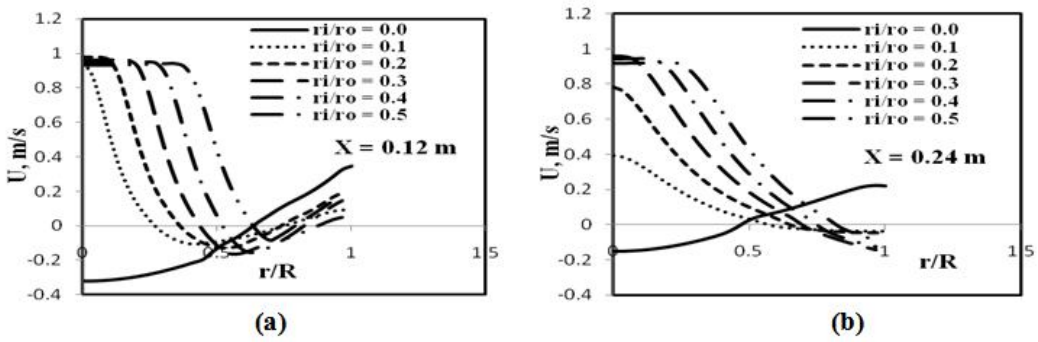

Figure 10, Velocity profiles at Different Ratio of Inlet Opening Radius to External Radius (Side Injection velocity, $V_{inj} = 0.02 m/s$).

4.3.3 Side Injection Velocity (V_{inj}) = -0.03 m/s

In this section the flow pattern has been analyzed at an injection velocity of -0.03 m/s. The r_i / r_o ratio has been varied and it has been seen that the size of the recirculation generated near the inlet of the duct gradually decreases. The r_i / r_o ratio is varied from 0.1 to 0.5. The velocity through the partially opened inlet is 1.0 m/s. The profiles of the axial velocity in fig. 12(a) and 12(b) confirms the same which shows the reduction of recirculation size with the increase of the r_i / r_o ratio. At X = 0.12 m, the axial velocity is positive at axis with an inlet opening and it is negative when the inlet is closed. The velocity profiles at any r_i / r_o ratio go negative at a certain radial location, but near the wall of the duct these profiles again go positive which confirms the generation of recirculation bubble within the axis and wall. At X = 0.24 m, the velocity profile near the wall is negative at r_i / r_o = 0.4 and 0.5 though these profiles are positive at X=0.12 m. So it can be said that at a constant side injection velocity with the increase of r_i / r_o ratio, the recirculation size reduces as well as it shifts towards the downstream from the inlet.

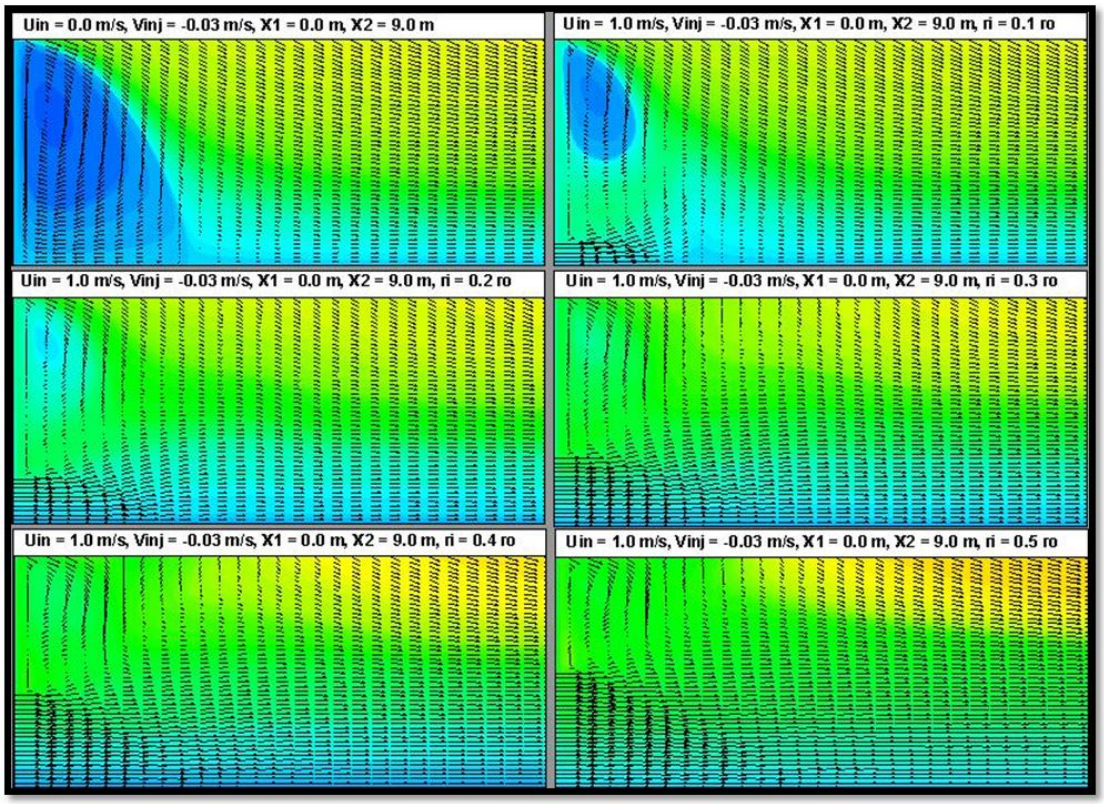

Figure 11, Variation of the Flow Pattern with the Changes of the Ratio of Inlet Opening Radius to the External Radius (Constant Side Injection Velocity, $V_{inj} = \mathbf{0.03} m/s$).

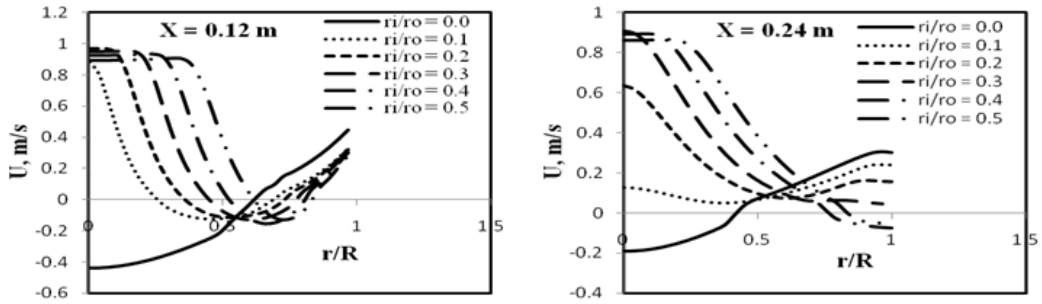

Figure 12, Velocity profiles at Different Ratio of Inlet Opening Radius to External Radius (Side Injection velocity, $V_{inj} = \mathbf{0.03} m/s$).

4.3.4 Side Injection Velocity (V_{inj}) = -0.08 m/s

Keeping the side injection velocity -0.08 m/s and inlet velocity through the partially opened inlet 1.0 m/s, the r_i / r_o ratio has been varied. The flow pattern and the onset of recirculatory flow have been shown in fig. 13 and the axial velocity profiles at different axial location has been shown in fig. 14(a) and

14(b). It is evident from the flow pattern that the size of recirculation zone decreases with the increase of r_i / r_o ratio and the velocity profiles also indicates the same findings. At X = 0.24 m, with a r_i / r_o of 0.3, 0.4 and 0.5, the axial velocity have total positive value but it have negative value at X = 0.12 m.

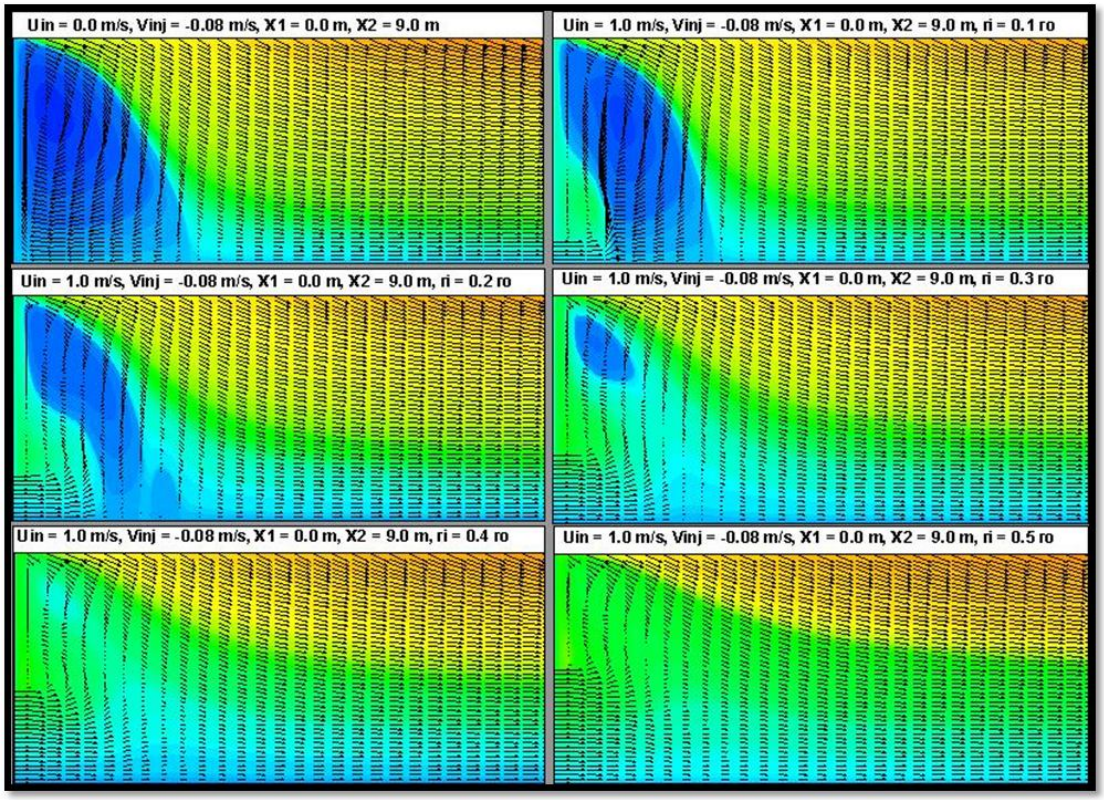

Figure 13, Variation of the Flow Pattern with the Changes of the Ratio of Inlet Opening Radius to the External Radius (Constant Side Injection Velocity, $V_{inj} = \mathbf{0.08} m/s$).

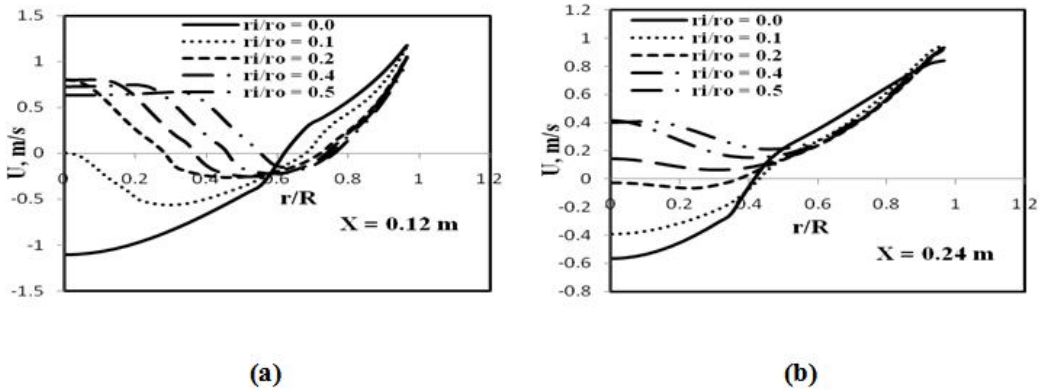

(a) **(b)**

Figure 14, Velocity profiles at Different Ratio of Inlet Opening Radius to External Radius (Side Injection velocity, $V_{inj} = \mathbf{0.08} m/s$).

4.3.5 Side Injection Velocity (V_{inj}) = 0.1 m/s

Fig. 15 shows the flooded streamline contour along with vector diagram revealing the onset of recirculation bubble and variation of its size with r_i / r_o ratio. The magnitude of r_i / r_o ratio determines the onset of the recirculation phenomenon. When the inlet of the duct is closed, the recirculation generated at the inlet and its depth is quite considerable from the axis to the wall of the duct. With an opening at inlet and turbulent fluid flow through the partially opened inlet at a velocity of 1.0 m/s, the size of the bubble gradually decreases. With the increase of this opening the recirculation bubble shifts from the inlet and its depth gradually decreases from the wall. In this case, the inlet flow can not overcome the momentum of side injection flow and the bubble is still present when the r_i / r_o ratio is 0.5.

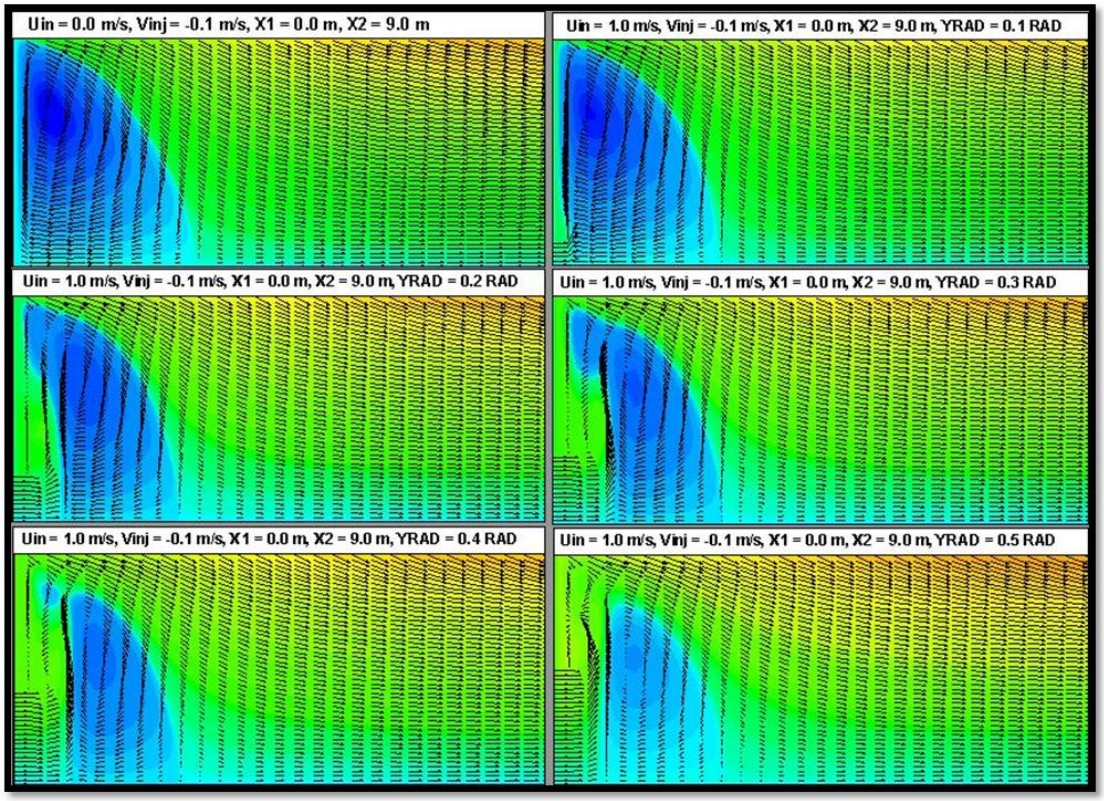

Figure 15, Variation of the Flow Pattern with the Changes of the Ratio of Inlet Opening Radius to the External Radius (Constant Side Injection Velocity, $V_{inj} = 0.1 m/s$).

Fig. 16(a) and 16(b) shows the velocity profiles at X = 0.12 m and X = 0.24 m. As the bubble shifts its location towards the downstream with increase of r_i / r_o ratio, the profiles of axial velocity goes further negative at X=0.24 m, in case of r_i / r_o = 0.3, 0.4, 0.5. With a bigger opening at inlet a larger mass

of fluid enters the duct, and thus the maximum negative value of axial velocity near axis at r_i / r_o=0.1, 0.2 reduced at X=0.24 m in comparison to the value at X=0.12 m.

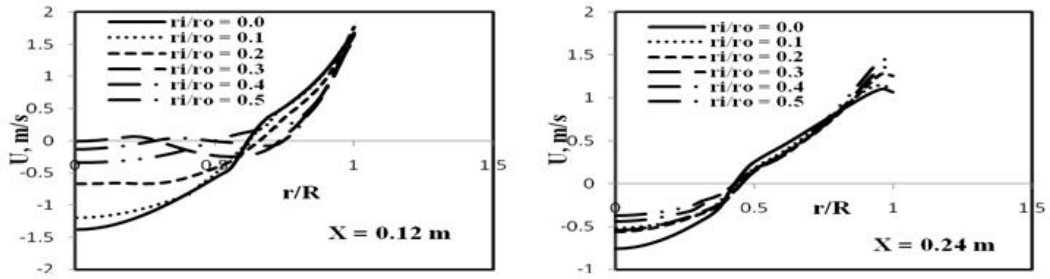

(a) **(b)**

Figure 16, Velocity profiles at Different Ratio of Inlet Opening Radius to External Radius (Side Injection velocity, V_{inj} **= 0.1***m / s*).

Fig. 17(a) and 17(b), shows the variation of recirculation length and depth with the ratio of inlet opening radius to external radius (r_i / r_o) for various injection velocity.

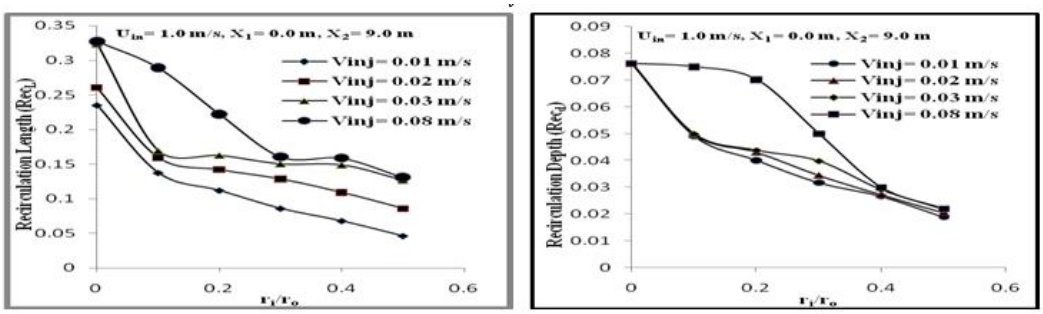

Fig. 17(a) **Fig. 17(b)**

Figure 17(a), Variation of Recirculation Length (Rec_L) with the Ratio of Inlet Opening Radius to External Radius (r_i/r_o) in a Partially Opened Enclosure. Figure 17(b), Variation of Recirculation Depth (Rec_d) with the Ratio of Inlet Opening Radius to External Radius (r_i/r_o) in a Partially Opened Enclosure.

It is evident from the plots that the recirculation length and depth decreases with the increase of r_i / r_o ratio. From fig. 17(a), it is shown that the length of the recirculation bubble depends on r_i / r_o ratio as well as the on the injection velocity. In case of flow through a porous duct with closed inlet when then injection velocity is -0.03 m/s and -0.08 m/s, the length of the bubble generated is around 0.325 m. But below these injection velocities the length of the bubble becomes smaller with injection velocity. In case of closed inlet the

depth of the recirculation bubble does not depend on the injection velocity which is depicted from fig. 17(b). In all the cases of injection velocities the depth of the bubble is around 0.08 m but with r_i / r_o it decreases.

CONCLUSIONS

The behavior of the flow of steady, incompressible turbulent fluid form the wall injection into a porous circular tube with closed and partially opened inlet has been carried out numerically. The flow pattern, onset of recirculation zone and its size has been investigated by varying the injection velocity in a closed duct. In a partially opened duct the r_i / r_o ratio has been varied along with the injection velocity to analyze the effect of inlet opening on the location and size of the low velocity flow reversal zone. The major conclusions of this work can be summarized as follows:

Due to the side mass injection in a closed duct, a recirculation generated at the inlet and its depth reaches from the axis to the wall of the duct. The length of the bubble increases with injection velocity and towards downstream there is no negative axial velocity.

Keeping injection velocity constant as the inlet of the duct opened partially by increasing the ratio of inlet opening radius (r_i) to the external radius of the duct (r_o), the recirculation bubble shifts its position from inlet to the downstream direction.

With the increase of inlet opening the size of the recirculation bubble gradually decreases and at a lower injection velocity at a certain opening it almost disappears.

ACKNOWLEDGEMENTS

The present study has been supported by the Council of Scientific and Industrial Research (CSIR).

NOMENCLATURE

C_μ	Empirical constant
C_t	Craya- Curtet number
D	Diameter of the cylindrical duct, m
f	Friction factor
G	Production term
K_1, K_2	Constants
L	Length of the cylindrical duct, m

Mr	Momentum ratio of side mass flow to the main axial flow
$\vec{n}$	Unit normal vector
Pd	Penetration Depth, m
R	Radius of the cylindrical duct, m
r	Radial co-ordinate across the duct
R_W	Recirculation Width, m
R_D	Recirculation Depth, m
R_c	Radius of curvature of the streamline
$\vec{s}$	Unit tangential vector
$\bar{u}$	Time mean velocity along *x*-axis, m/s
U_{in}	Inlet flow velocity, m/s
U_{mean}	Mass-averaged mean axial velocity, m/s
$\bar{v}$	Time mean velocity along *y*-axis, m/s
V_{inj}	Side injection velocity, m/s
X	Axial co-ordinate along the duct, m
Re	Reynolds Number = $\frac{\rho v D}{\mu}$
ε	Turbulent dissipation rate, m^2/s^3
k	Turbulent kinetic energy, m^2/s^2
μ	Viscosity of the air, kg/m-s
μ_{eff}	Effective viscosity, kg/m-s
μ_l	Laminar viscosity, kg/m-s
μ_t	Eddy viscosity, kg/m-s
ψ	Stream function, m^2/s
ρ	Density of air, kg/m^3

REFERENCES

[1] S.W. Yuan and E.W. Brogren,(1961), Turbulent Flow in a Circular Pipe with Porous Wall, *Phys. Of Fluids*, 4, pp. 368-372.

[2] M. Barchilon and R. Curet, (1964), Some Details of the Structure of an Axi-Symmetric Confined Jet With Backflow, *Trans. ASME, J. Basic Engg.* 86, pp. 777-786.

[3] R. M. Olson, and E. R. G. Eckert, (1966), Experimental Studies of Turbulent Flow in a Porous Circular Tube with Uniform Fluid Injection through the Tube Wall, *J. Appl. Mech.*, March, pp. 7-17.

[4] B. E. Launder, D. B. Spalding, (1974), The Numerical Computation of Turbulent Flows, *Comput. Methods in Appl. Mech.* 3 (1974), pp. 269-289.

[5] M. A. Leschziner and W. Rodi, (1981), Calculation of Annular and Twin Parallel Jets UsingVarious discretization Schemes and Turbulence-Model Variations, *Trans. ASME, J. Fluids Engg*. 103, pp. 352-360.

[6] S. V. Patankar, (1981), Numerical Heat Transfer and Fluid Flow, McGraw-Hill, New York.

[7] R. A. Beddini, (1986), Injection Induced Flows in Porous Walled-Ducts, *AIAAA J.* 24, pp. 1766-1773.

[8] Y Sumitani, N Kasagi, (1995), Direct Numerical Simulation of Turbulent Transport with Uniform Wall Injection and Suction, *AIAA J.* 33, pp. 1220-1228.

[9] G. Casalis, G. Avalon, J.P. Pineau, (1998), Spatial Instability of Planar Channel Flow with Fluid Injection through Porous Wall, *Phys. of Fluids.* 10, pp. 2558-2568.

[10] M. Ali, T. Fujiwara, J.E. Lablanc, (2000), Influence of Main Flow Inlet Configuration on Mixing and Flame Holding in Transverse Injection into Supersonic Air Stream, *Int. J. of Engg. Science.* 38, pp. 1161-1180.

[11] T. Feraille, G. Casalis, (2003), Channel Flow Induced by Wall Injection of Fluid and Particles, *Phys. of Fluids.* 15, pp. 348-360.

[12] S. V. Apte and V. Yang, (2003), A Large Eddy Simulation Study of Transition and low Instability in a Porous Walled Chamber with Mass Injection, *J. Fluid Mech.* 477, pp. 215-225.

[13] R. Knikker, M. Michard, G. Bois, (2008), Numerical Study of Buoyancy Effects in a Channel Flow Generated by a Symmetric Wall Injection, *5th European Thermal Science Conference*, The Netherlands. (2008).

[14] S. Majumder, D. Sanyal, (2008) Destabilization of Laminar Wall Jet Flow and Re-Laminarization of the Turbulent Confined Jet Flow in Axially Rotating Circular Pipe, Trans. ASME, J. of Fluid Engg, 130, pp. 011203-1 – 011203-8.

[15] C. Fournier, M. Michard, F. Bataille, (2010), Experimental Investigations of an Internal Flow Generated by Porous Injection, *ASME, J.ofAppl.Mech.*7,pp.1577-1585.